DISCONTINUOUS GALERKIN METHOD FOR DUCT ACOUSTICS

Carl P.A. Blom, Rob Hagmeijer, Harry W.M. Hoeijmakers
***Group Engineering Fluid Dynamics, University of Twente, the Netherlands**

Keywords: *Discontinuous Galerkin, Computational Aeroacoustics, Duct Acoustics*

Abstract

In the present paper analytical and numerical results obtained for the problem of acoustic radiation from a vibrating wall segment inside an infinite rectangular duct with uniform mean flow are presented and compared. The numerical results are obtained employing a recently developed Discontinuous Galerkin finite element method implemented on a tetrahedral grid.

The presented leading term in the analytical solution, which represents a propagating plane wave, is shown to capture most of the characteristics of the solution. For the plane wave a closed form solution is presented for two specific wall vibration velocities. The remainder of the analytical solution is given by an infinite number of 'diffracted waves' (waves affected by reflection, scattering, diffraction, etc.). For the diffracted waves, which are decaying modes, only an approximate solution has been obtained employing the method of stationary phase. Only near the vibrating wall segment the influence of the diffracted waves is shown to be significant.

The presented numerical and analytical results are shown to be in very good agreement.

1 Introduction

Computational Aeroacoustics (CAA) is a rapidly growing branch in fluid mechanics. One of the driving forces behind the rapid growth may be the governmental policies on the reduction of sound emissions. This relates especially to the noise produced by aircraft, but also trucks, cars (highways), trains etc. Much of the advance has also been driven by the availability of more powerful computational resources and the availability of aeroacoustic test facilities.

Numerical methods introduce artificial dissipation and dispersion. Numerical dissipation unphysically dampens the vibration amplitude of the sound waves and numerical dispersion alters the propagation speed in an unphysical manner. The longer the propagation distances and the higher the frequencies involved the more apparent these unphysical influences become. Higher-order methods, higher than the usually first or second-order Computational Fluid Dynamics (CFD) methods, can be used to remedy these problems.

A Discontinuous Galerkin (DG) method has been developed for the accurate simulation of the propagation of acoustic information through fluids moving with non-uniform velocity in three-dimensional complex domains. The DG method is an extremely compact finite element method which is applicable to both structured and unstructured meshes and which can be extended to higher-order accuracy relatively easily.

In the present paper numerical results obtained for the acoustic radiation from a vibrating wall segment inside an infinite rectangular duct are presented. The objective is to compare numerical and analytical results in order to identify the relevant phenomena and to verify the numerical algorithm employed. The analytical solution for this problem has been presented in Blom [2] and will only be summarized here.

2 Discontinuous Galerkin Method for the Linearized Euler Equations

2.1 Linearized Euler Equations

Assuming that there is no significant feedback (or back-reaction) of the sound field to the mean flow, it is widely recognized that the propagation of sound can be described by the linearized Euler equations (LEE). Assuming that the background flow satisfies the homogeneous Euler equations in three spatial dimensions and that we are dealing with a calorically perfect gas, the LEE for the primitive perturbation variables $\mathbf{u} = (\rho, u, v, w, p)^T$, where ρ denotes the density perturbation, u, v, and w denote the three perturbation velocity components and p denotes the pressure perturbation, can be written as:

$$\frac{\partial \mathbf{u}}{\partial t} + \frac{\partial \mathbf{f}_j}{\partial x_j} + D_0 \mathbf{u} = \mathbf{s}, \quad \mathbf{f}_j \equiv A_{j0}\mathbf{u}, \tag{1}$$

where $j = 1, 2, 3$, and where

$$A_{j0} = \begin{bmatrix} u_{j0} & \delta_{1j}\rho_0 & \delta_{2j}\rho_0 & \delta_{3j}\rho_0 & 0 \\ 0 & u_{j0} & 0 & 0 & \frac{\delta_{1j}}{\rho_0} \\ 0 & 0 & u_{j0} & 0 & \frac{\delta_{2j}}{\rho_0} \\ 0 & 0 & 0 & u_{j0} & \frac{\delta_{3j}}{\rho_0} \\ 0 & \gamma\delta_{1j}p_0 & \gamma\delta_{2j}p_0 & \gamma\delta_{3j}p_0 & u_{j0} \end{bmatrix}, \tag{2}$$

where γ is the ratio of specific heats. The respective entries of the matrix A_{j0} depend only on one of the components (and not on products) of the background or mean flow vector $\mathbf{u}_0 = (\rho_0, u_0, v_0, w_0, p_0)^T$. Furthermore:

$$D_0 \equiv C_0 - \frac{\partial A_{j0}}{\partial x_j}, \tag{3}$$

where

$$C_0 = \begin{bmatrix} \frac{\partial u_{j0}}{\partial x_j} & \frac{\partial \rho_0}{\partial x} & \frac{\partial \rho_0}{\partial y} & \frac{\partial \rho_0}{\partial z} & 0 \\ \frac{-1}{\rho_0^2}\frac{\partial p_0}{\partial x} & \frac{\partial u_0}{\partial x} & \frac{\partial u_0}{\partial y} & \frac{\partial u_0}{\partial z} & 0 \\ \frac{-1}{\rho_0^2}\frac{\partial p_0}{\partial y} & \frac{\partial v_0}{\partial x} & \frac{\partial v_0}{\partial y} & \frac{\partial v_0}{\partial z} & 0 \\ \frac{-1}{\rho_0^2}\frac{\partial p_0}{\partial z} & \frac{\partial w_0}{\partial x} & \frac{\partial w_0}{\partial y} & \frac{\partial w_0}{\partial z} & 0 \\ 0 & \frac{\partial p_0}{\partial x} & \frac{\partial p_0}{\partial y} & \frac{\partial p_0}{\partial z} & \gamma\frac{\partial u_{j0}}{\partial x_j} \end{bmatrix}. \tag{4}$$

The entries of the matrix D_0 are linear in the components of the gradients $\frac{\partial \mathbf{u}_0}{\partial x_j}$. The acoustic source vector $\mathbf{s}$ in Eq.(1) can be used to describe complex processes which result in perturbations of the primitive perturbation variables.

In the subsequent sections it is assumed, for simplicity, that the background flow is uniform, which results in $D_0 = 0$. In addition the LEE are used in dimensionless form. To obtain dimensionless quantities densities are scaled with ρ_{ref}, lengths with L, time with L/c_{ref} and pressure with $\rho_{ref}c_{ref}^2$, where ρ_{ref}, c_{ref} and L are an appropriate reference density, velocity and length scale, respectively.

2.2 Discontinuous Galerkin Method

The Discontinuous Galerkin (DG) method is an extremely compact finite element method which is applicable to both structured and unstructured meshes. The solution is approximated by a local polynomial expansion in each element of the computational mesh and the solution is not required to be continuous over element interfaces. The size of the computational stencil is independent of the desired order of the method. DG methods of arbitrarily high formal accuracy can be obtained by suitably choosing the degree of the approximating polynomials. Because of the compactness of the scheme, it is highly parallelizable, it is very well suited for handling complex geometries and allows for a relatively simple treatment of the boundary conditions. Therefore the DG method is very well suited for application to the simulation of the propagation of acoustic information in fluids moving at non-uniform velocity in three-dimensional complex domains.

A detailed description of the DG method is given in Blom [2] and can also be found in a.o. Atkins & Shu [1]. In the present work we will only present the final result. To this end, let us consider the Linearized Euler equations (LEE) on the domain Ω which we partition into N_e non-overlapping elements Ω_j, $j = 1, 2, \ldots, N_e$. The DG spatial discretization of the LEE in each ele-

ment Ω_j can then be written as:

$$\int_{\Omega_j} \frac{\partial \mathbf{u}_h}{\partial t} b_{jm} d\Omega - \int_{\Omega_j} \mathbf{f}_i(\mathbf{u}_h) \frac{\partial b_{jm}}{\partial x_i} d\Omega + \sum_{l \in I_j} \int_{\partial\Omega_{jl}} \mathbf{h}(\mathbf{u}_j, \mathbf{u}_l, \mathbf{n}_j) b_{jm} d\Gamma = \int_{\Omega_j} \mathbf{s} b_{jm} d\Omega \tag{5}$$

where $\mathbf{u}_h$ is the approximation of the solution $\mathbf{u}$ given by:

$$\mathbf{u}_h(\mathbf{x},t) = \sum_{j=1}^{N_e} \sum_{k=0}^{M} \mathbf{v}_{jk}(t) b_{jk}(\mathbf{x}), \tag{6}$$

k and m (Eq.(5)) are indices over the basis functions and $I_j = \{k_1, k_2, k_3, k_4\}$ is the set of global indices, describing the direct-neighborhood-elements Ω_{k_l} of element Ω_j, $j \notin I_j$ and $l \in I_j$ when $\partial\Omega_j \cap \partial\Omega_l \neq 0$ $(l \neq j)$. In the present work the local Lax-Friedrichs flux:

$$\mathbf{h}(\mathbf{u}_j, \mathbf{u}_l, \mathbf{n}_j) = \frac{1}{2}\left(\mathbf{f}^n(\mathbf{u}_j) + \mathbf{f}^n(\mathbf{u}_l)\right) - \frac{1}{2}\alpha\left(\mathbf{u}_l - \mathbf{u}_j\right)$$
$$\mathbf{f}^n(\mathbf{u}_j) = (n_j A_j)\mathbf{u}_j, \tag{7}$$

provides the crucial coupling and handles the discontinuity at element interfaces.

In Eq.(6), and therefore also in Eq.(5), $\mathbf{v}_{jk}(t)$ are the unknowns (vectors containing five elements). The unknowns are marched in time employing a four-stage low-storage Runge-Kutta algorithm.

3 Acoustic Radiation from Vibrating Wall Segment Inside Infinite Rectangular Duct

3.1 Problem Description

Consider an infinite rectangular duct of height $h = 1$ and width b, see Fig.(1). In the bottom wall of the duct a finite part, of length $2l$ and width b, is allowed to vibrate. The origin of the Cartesian coordinate system is in the mid-section of the vibrating segment of the duct at one of the lower corners. In the origin we define the orthogonal unit coordinate vectors $\mathbf{e}_x, \mathbf{e}_y$ and $\mathbf{e}_z$. In the present paper we consider the perturbation field generated by the vibrating wall segment inside the infinite duct. It is assumed that the problem can be described by the linearized Euler equations (LEE; see also section 2.1), which are non-dimensionalized employing the speed of sound in the undisturbed flow c_0, the height h of the duct and the density of the undisturbed flow ρ_0. For the mean flow velocities, expressed in terms of Mach numbers, we assume $\mathbf{u}_0 = (M, 0, 0)^T$. In addition, we assume that the amplitude of

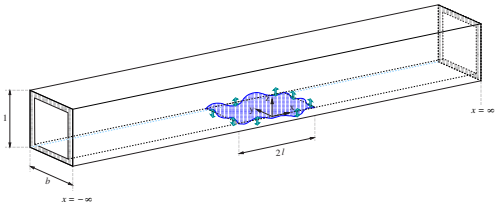

Fig. 1 Infinite rectangular duct with vibrating wall segment.

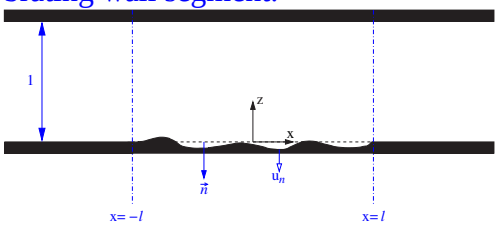

Fig. 2 Side view of vibrating wall segment.

the wall displacement is small compared to the acoustic wave length, $\tilde{\lambda}$, the surface dimensions, $2l$ and b, and the height of the duct $h = 1$. Based on these assumptions it is consistent to linearize the boundary condition associated with the moving surface z_s with respect to the stationary reference surface $z = 0$ (Pierce [9]). The motion of the surface $z = z_s(x,y,t)$, with $z_s \ll b$, $z_s \ll l$, $z_s \ll h = 1$ and $z_s \ll \tilde{\lambda}$, leads to a normal velocity boundary condition for the LEE for $z = 0$:

$$u_n(x,y,t) = \psi(x,y,t) H(l - |x|), \tag{8}$$

where

$$\psi(x,y,t) = -\left(\frac{\partial z_s}{\partial t} + M\frac{\partial z_s}{\partial x}\right), \tag{9}$$

and H is the Heaviside function.

From the LEE the convected wave equation can be derived for the pressure:

$$\frac{D^2p}{Dt^2} - \frac{\partial^2 p}{\partial x_j \partial x_j} = 0, \quad \frac{D}{Dt} \equiv \frac{\partial}{\partial t} + M\frac{\partial}{\partial x}. \qquad (10)$$

Taking the inner product of the momentum equation with the unit normal $\mathbf{n}_0 = -\mathbf{e}_z$ and linearizing with respect to $z = 0$ and small $\frac{\partial z_s}{\partial x}$, $\frac{\partial z_s}{\partial y}$, results in the following linearized boundary condition for the pressure at $z = 0$:

$$\frac{\partial p}{\partial z}\Big|_{z=0} = \frac{\partial u_n}{\partial t} + M\frac{\partial u_n}{\partial x}. \qquad (11)$$

On the other walls, which are rigid, we apply hard-wall boundary conditions.

3.2 Analytical Solution

The mathematical procedure used to obtain the analytical solution is based on the procedure presented by Kuijpers, Rienstra, Verbeek & Verheij [6], who developed a mathematical model for the acoustic radiation in baffled cylindrical ducts of finite length. The mathematical procedure combines the techniques of separation of variables, Fourier transformation, Fourier series expansion and complex integration and is used here to solve the problem introduced in the previous (sub-) section. In Kuijpers et al. [6] the solution is provided for the wall vibration inside a cylindrical duct of finite length, the mean flow is absent and the solution is presented in the frequency domain. In contrast, we derived an analytical solution in the time domain, for an infinitely long rectangular duct, while we consider cases with and without uniform mean flow. Although in numerous textbooks, such as Crighton [4], Morse & Ingard [8] and Pierce [9], but also Jones [5] and Morse & Feshbach [7], the subject of propagation and diffraction of sound waves in ducts is covered, the vibration of a finite part of the wall that radiates sound into the rectangular duct has, to the author's knowledge, not been considered as such.

In the present paper we consider two specific wall vibration velocity functions, one describing a plunging wall segment and the other describing spatial vibration modes in axial direction. For these specific choices the analytic solution for the pressure perturbation in the time domain can be derived explicitly for the leading term of the solution. A brief description of the solution procedure has been presented in a recent paper by Blom et al. [3]. A detailed description can be found in Blom [2].

3.3 Case A: Plunging wall segment

Let us assume for ψ in Eq.(8) the following function:

$$\psi(x,y,t) = \psi^A(t) = \sin(\omega_0 t)e^{-at}H(t), \qquad (12)$$

where $a \geq 0$ and where H is the Heaviside function. In this case the entire plate ($-l \leq x \leq l$) moves up and down as a rigid body. For $a > 0$ the amplitude of the introduced vibration of the wall is exponentially damped because of the exponential term in Eq.(12).

The pressure in the time domain, which becomes independent of the y-coordinate for the present problem, can be written as:

$$p^A(x,z,t) = p_0^A(x,t) + \sum_{k=1}^{\infty} \cos(\beta_k z) p_k^A(x,t), \qquad (13)$$

where $\beta_k = k\pi$ and (see Blom [2] for a detailed derivation):

$$p_0^A(x,t) = \frac{1}{2}\frac{\omega_0}{\omega_0^2 + a^2}\Big\{g^A(\tau_1)H(\tau_1) - g^A(\tau_2)H(\tau_2)\Big\}, \qquad (14)$$

where

$$g^A(\tau) = \left[\cos(\omega_0\tau) + \frac{a}{\omega_0}\sin(\omega_0\tau)\right]e^{-a\tau} - 1, \qquad (15)$$

$$\tau_{1,2} = t - \frac{x \mp l}{1+M}, \qquad (16)$$

τ is the so-called retarded or emission time, the time at which the signal, which has been emitted at $t = 0$, is observed at location x and time t. For p_k^A,

$$p_k^A(x,t) = \frac{-\omega_0}{2\pi i}\int_{-\infty}^{\infty} \frac{[e^{-i(x-l)\Lambda_{0k}} - e^{-i(x+l)\Lambda_{0k}}]e^{i\omega t}d\omega}{\omega[i(\omega-\omega_0)+a][i(\omega+\omega_0)+a]}, \qquad (17)$$

$$\Lambda_{0k} \equiv \frac{\sqrt{\omega^2 - (1-M^2)\beta_k^2}}{1-M^2}, \qquad (18)$$

no closed form solution has been found.

It is observed from Eq.(17) and Eq.(18) that for k such that $(1-M^2)\beta_k^2 > \omega^2$ the integrand decreases at an increasing rate when $x > l$ becomes larger. Apparently a large (infinite) number of modes is exponentially decaying or so-called cut-off. These specific waves or modes are also known as evanescent waves or decaying modes. Considering the integrand in Eq.(17) we observe that for $\omega = \pm\beta_k$ we have branch points, which greatly complicate the evaluation of p_k^A. Integrals of the form of Eq.(17) are called diffraction integrals by Crighton et al. [4], because they often appear in diffraction problems. The pressure perturbations p_k^A represent waves affected by reflection, scattering, diffraction, etc. However, upon employing the method of stationary phase (e.g. Crighton et al. [4]) an approximate solution can be found assuming both $x \pm l$ and t large, with $t > x \pm l$, see also Blom [2].

3.4 Case B: Spatial vibration modes

Let us now consider for ψ in Eq.(8) the function:

$$\psi^B(x,t) = \cos(\chi_n x)\sin(\omega_0 t)H(t), \qquad (19)$$

where

$$\chi_n = \frac{n\pi}{2l}, \quad n \in \mathbb{N}, \quad n \text{ odd}. \qquad (20)$$

As in the previous section, section 3.3, the solution is independent of y and can be written in the form of Eq.(13):

$$p^B(x,z,t) = p_0^B(x,t) + \sum_{k=1}^{\infty} \cos(k\pi z) p_k^B(x,t). \qquad (21)$$

For p_k^B, as for p_k^A, no closed form solution has been found. However, as for Case A an approximate solution can be obtained employing the method of stationary phase. We will here only present the final result for p_0^B.

$$p_0^B(x,t) = \frac{-\sin(\chi_n l)}{2(\chi_n^2 - \omega_0^2)} \Big\{ g^B(\tau_1)H(\tau_1) \qquad (22)$$

$$+ g^B(\tau_2)H(\tau_2) \Big\}, \qquad (23)$$

where $\sin(\chi_n l) = (-1)^{\frac{n-1}{2}}$ and

$$g^B(\tau) = \omega_0 \sin(\chi_n \tau) - \chi_n \sin(\omega_0 \tau). \qquad (24)$$

The retarded times $\tau_{1,2}$ are given by Eq.(16).

4 Results

In the numerical simulations a finite duct is considered. At the end planes of the duct, which are located sufficiently far away from the vibrating wall segment, we apply so-called characteristic non-reflecting boundary conditions. On the other walls, except for the vibrating part, we apply hard-wall boundary conditions. At the vibrating wall the mean flow velocity normal to the wall is zero, the normal velocity for the perturbation field is prescribed and given by ψ.

When the mean flow is absent, the problem is symmetric with respect to the plane $x = 0$, which has also been verified numerically. For $M = 0$ the dimensionless linearized Euler equations are solved in a rectangular domain, given by $x \in [0, x_{max}]$, $y \in [0,1]$ and $z \in [0,1]$, where all lengths are non-dimensional. For $M \neq 0$ the problem is no longer symmetric with respect to the $x = 0$-plane and the linearized Euler equations are solved in the domain $x \in [-x_{max}, x_{max}]$, $y = [0,1]$ and $z = [0,1]$. In most cases $x_{max} = 40$.

In order to obtain the tetrahedral computational grid, the physical domain is first partitioned into equally sized cubes, each of which is subsequently divided into twelve identical tetrahedrons. In this way a regular type of tetrahedral mesh is obtained. For the problems considered, a grid-convergence study has been conducted. In most cases for $M = 0$ a mesh containing 60000 elements was found sufficient. For $M \neq 0$ a mesh containing 120000 elements was found adequate. During the computations the results are evaluated in all nodes of the tetrahedral grid. In addition, a time history of the perturbation variables is recorded at certain specific locations in the rectangular duct. We will refer to these locations as 'microphone' (mic) locations.

4.1 Case A, $M = 0$

For the plunging wall segment without mean flow we present results for three different combinations of the parameters ω_0, l and a.

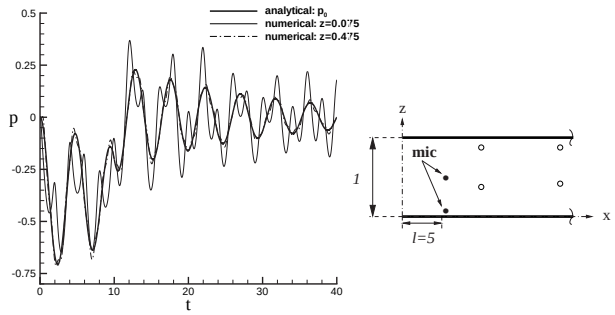

Fig. 3 Results at $x = 5.025$, for $M = 0$, $\omega_0 = \frac{4}{3}$, $l = 5$ and $a = 0.05$.

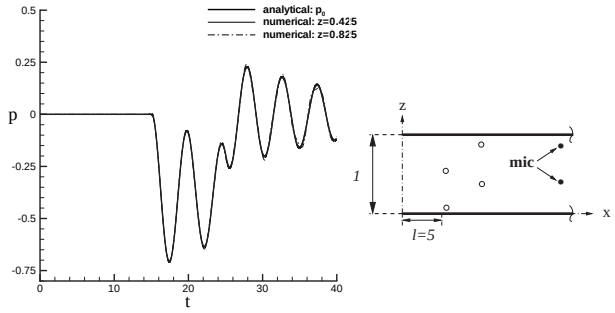

Fig. 4 Results $x = 20.075$, for $M = 0$, $\omega_0 = \frac{4}{3}$, $l = 5$ and $a = 0.05$.

Result for $\omega_0 = \frac{3}{4}$, $l = 5$, $a = 0.05$: In Figs.(3) and (4) numerical results and the p_0^A-part of the analytical solution are shown for $\omega_0 = \frac{4}{3}$, $l = 5$ and $a = 0.05$. Fig.(3) shows time histories of the pressure perturbations obtained very close to the vibrating wall. In the figure, two numerical results are presented, obtained at two z-locations, viz. $z = 0.075$ and $z = 0.475$, respectively. At $z = 0.475$ the difference between the p_0^A-part of the analytical solution and the numerical result for p is observed to be relatively small. At $z = 0.075$ the difference is observed to be significant. This can be explained by the fact that for $z = \frac{1}{2}$ the term $\cos(\beta_k z)$ in Eq.(13) becomes zero when k is uneven. At the end of section 3.3 it was argued ($M = 0$) that for k such that $\beta_k > \omega$ we are dealing with decaying modes. It is furthermore expected that $|p_1^A| > |p_2^A| > \ldots > |p_\infty^A|$ and that for $k \to \infty$ we have $|p_k^A| \to 0$. From the results shown in Fig.(3) it appears that the contribution of $p_0^A(x,t)$ and $\cos(\pi z)p_1^A(x,t)$ to the solution are most dominant. When the microphone is located near the vibrating wall and not near $z = \frac{1}{2}$ the contribution of $p_k^A(x,z,t)$ to the solution cannot be neglected.

In Fig.(4) results are shown in the plane $x = 20.075$. The difference between the numerical result at $z = 0.425$ and p_0^A is now no longer distinguishable. Even at $z = 0.825$ the numerical result is observed to deviate very little from p_0^A. From these results, as well as other results shown in Blom [2], it is concluded that with increasing distance from the vibrating wall segment, the result for the pressure p^A gets increasingly better approximated by the analytical solution p_0^A.

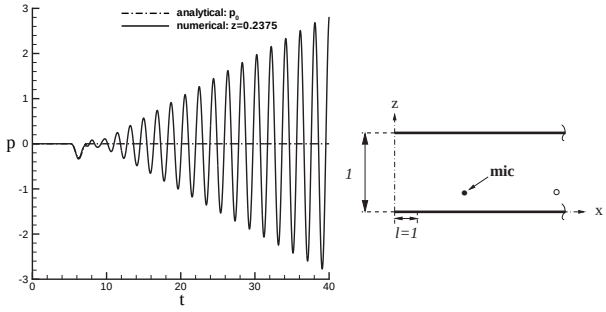

Fig. 5 Results at $x = 6.2625$, for $M = 0$, $\omega_0 = \pi$, $l = 1$ and $a = 0$.

Result for $\omega_0 = \pi$, $l = 1$, $a = 0$: When the angular wall vibration frequency ω_0 is chosen equal to $n\pi$, $n \in \mathbb{N}^+$, the perturbation created by the plunging wall travelling from $z = 0$ to $z = 1$, will have a wave length $\tilde{\lambda}$ of $2n$-times the duct height, i.e. $\tilde{\lambda} = 2n$. It is well known from literature that in such cases the pressure will increase without limit (in reality at least as long as linear theory is valid), in other words we are dealing with resonance.

In Fig.(5) the numerical result and p_0^A-part of the analytical solution are presented at the microphone location $x = 6.2625$, $y = 0.5125$ and $z = 0.2375$ for $\omega_0 = \pi$, $l = 1$ and $a = 0$. Clearly the numerical solution is observed to have an amplitude that grows linearly in time, as expected.

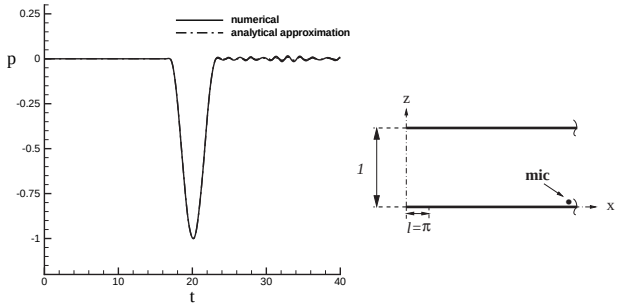

Fig. 6 Results at location $x = 20.101$, $y = 0.525$ and $z = 0.025$ for $M = 0$, $\omega_0 = 1$, $l = \pi$ and $a = 0$. Analytic approximation for p_k^A is obtained from applying the method of stationary phase.

Result for $\omega_0 = 1$, $l = \pi$, $a = 0$: The frequency of the function g^A, which is present in the expression for p_0^A and given by Eq.(15), clearly depends on the vibration frequency ω_0, as we have seen above. The frequency of the solution p_0^A, however, also depends on the (dimensionless) length $2l$ of the vibrating wall. At a certain microphone location x, the signal from the left end of the vibrating wall follows the signal from the right end of the vibrating wall $2l$ dimensionless time-units later. Therefore, depending on the length $2l$, the two signals can amplify each other maximally, cancel each other or anything in between.

An extreme example of the influence of the length of the vibrating wall on the pressure perturbation is presented in Fig.(6), which shows the result for $\omega_0 = 1$, $l = \pi$ and $a = 0$. For this specific choice of the parameters the analytic solution for p_0^A only shows one major 'pulse' of width 2π. For $a = 0$ and $l = \pi$ the contribution from the right and the left end of the vibrating wall cancel each other for $t \geq x + l$ (independent of ω_0). In the figure the pulse is given by the contribution from the right end of the vibrating wall, as soon as the contribution from the left end of the vibrating wall reaches the microphone position ($t = x + l$) the two signals cancel each other. From this time on only the contribution to the solution from the p_k^A-terms is visible. This specific choice of parameters provides a perfect opportunity to compare the numerical solution with the analytical approximation for p_k^A given by the method of stationary phase.

From Fig.(6) it is observed that the analytical approximation to p^A shows very good agreement with the numerical result. A magnification of the results for $t > x + l$, when p_0^A is zero, revealed that the analytical approximation slightly underpredicts the amplitude, but the frequency is well resolved.

In Fig.(7) contour plots in the plane $y = 0.5$ for the pressure perturbation at dimensionless times $t = 5$, 10, 15, 20, 25, and $t = 30$ are presented. Only pressure perturbation levels between -0.01 and 0.01 are shown, i.e. every value above $p = 0.01$ is white, every value below $p = -0.01$ is black. Next to each contour plot of Fig.(7) there is a figure showing the pressure perturbation $p(x, 0.5, 0.25, t_i)$ obtained for the same dimensionless time, t_i, and for $x \in [0, 40]$. The plotting levels in these figures have been adjusted to capture the minimum and maximum pressure perturbation in the duct.

In Fig.(7) the pressure perturbation given by p_0 is presented by the black band of width 2π which moves to the right with increasing time. At these pressure levels it is clearly observed that the pressure fluctuations given by p_k^A form an antisymmetric pattern with respect to $z = \frac{1}{2}$ in the duct. It is furthermore observed that at greater distances from the vibrating wall the amplitude of the pressure perturbations given by p_k^A decreases.

4.2 Case A, $M \neq 0$

Fig.(8) shows numerical and analytical results for four different Mach-numbers, i.e. $M = 0.05$, 0.1 0.2 and 0.4, at location $x = 20.025$, $y = 0.525$ and $z = 0.475$. The numerical result is within plotting accuracy identical to the analytical result.

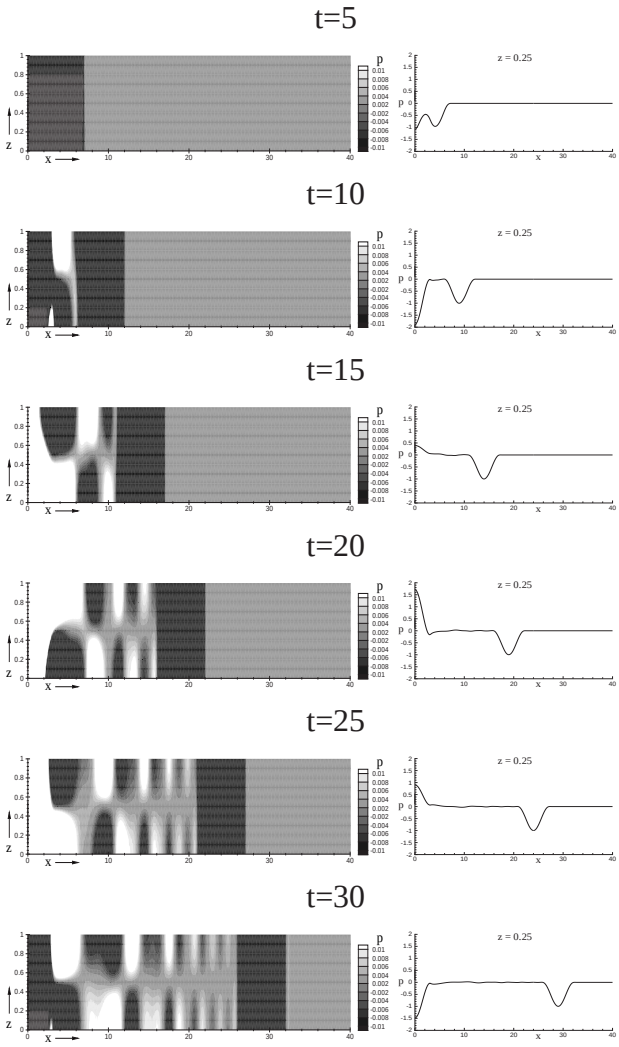

Fig. 7 Case A: $l = \pi$, $\omega_0 = 1$ and $a = 0$. Left: Contour plots for the pressure perturbation in the plane $y = 0.5$. Right: Pressure perturbation for $y = 0.5$ and $z = 0.25$. Note the large difference in plotting scales for the pressure.

From Fig.(8) it is clear that with increasing mean flow velocity M, the signal from the vibrating wall reaches the microphone earlier, as expected and also predicted by the analytic solution p_0^A, Eq.(14). In addition it is observed that with increasing M also the amplitude decreases. The observed frequency of the signal, however, is not changed. Although not many parameters have been varied for the plunging wall case with mean flow, it has been shown convincingly that

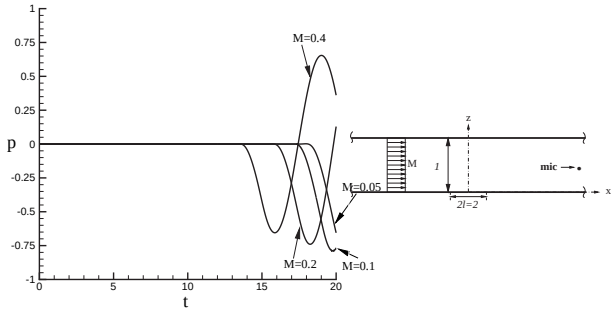

Fig. 8 Numerical and analytical results for Case A for four different Mach-numbers, showing influence of Mach-number on the retarded time at location $x = 20.025$, $y = 0.525$ and $z = 0.475$. Parameters: $\omega_0 = 1$, $l = 1$ and $a = 0$.

also for the case including mean flow the numerical results and the analytical prediction of p_0^A are in very good agreement.

4.3 Case B, $M = 0$

In the problem of Case B (see also section 3.4), there are three parameters which may be varied, i.e. the length of the vibrating part of the wall $2l$, the angular frequency of the vibration ω_0 and the frequency of the wall motion $\chi_n = \frac{n\pi}{2l}$ (n odd), see also Eq.(19).

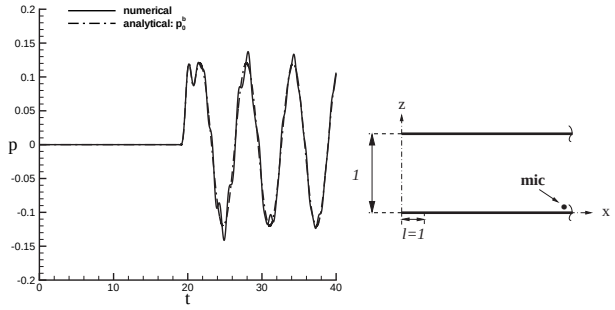

Fig. 9 Results for Case B at location $x = 20.075$, $y = 0.525$ and $z = 0.025$ for $l = 1$ and, $\omega_0 = 1$ and $\chi_3 = \frac{3\pi}{2}$.

The solution for Case B has been observed to depend on the parameters ω_0 and l in a similar

fashion as the solution of Case A, described in the previous section.

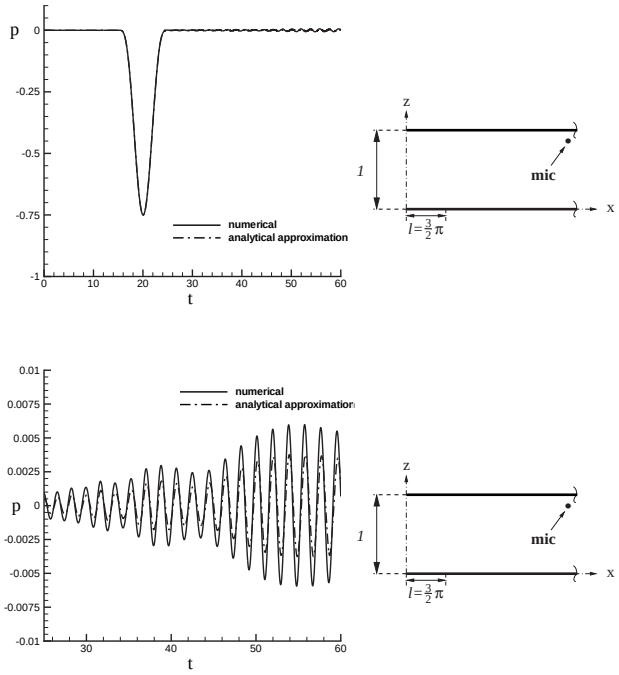

Fig. 10 Results for Case B at location $x = 20.0522$, $y = 0.475$ and $z = 0.725$ for $l = \frac{3}{2}\pi$, $\omega_0 = 1$ and $\chi_1 = \frac{1}{3}$. Analytical approximation for p_k^B is obtained from applying the method of stationary phase. Bottom: Magnification for $t \in [25, 60]$.

Result for $\omega_0 = 1$, $l = 1$ and $\chi_3 = \frac{3\pi}{2}$: In Fig.(9) results for Case B for $\omega_0 = 1$, $l = 1$ and $\chi_n = \frac{3\pi}{2}$, so $n = 1$, at microphone location $x = 20.075$, $y = 0.525$ and $z = 0.025$ are presented.

For $\chi_n = \frac{\pi}{2}$ (not shown) the numerical result was observed to be in very good agreement with the analytical solution for p_0^B, given by Eq.(22). In Fig.(9) a slight difference between the numerical result and p_0^B can be observed. This is thought to be caused by the contribution of p_k^B, which has not been included in the presented analytical solution. For $\chi_n = \frac{5\pi}{2}$ (also not shown) the observed difference between the numerical result and p_0^B increased a little. Especially in the first dimensionless time units after the signal has reached the microphone, rapid oscillations around p_0^B are observed. For $\chi_n = \frac{5\pi}{2}$ these oscillations are more

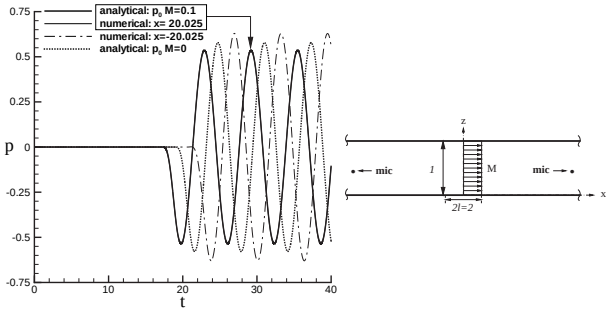

Fig. 11 Numerical result and analytical solution $p0$ for Case B at locations $x = \pm 20.025$, both at $y = 0.525$ and $z = 0.475$. Parameters: $\omega_0 = 1$, $l = 1$, $\chi_1 = \frac{1}{2}$ and $M = 0.1$.

rapid than for $\chi_n = \frac{3\pi}{2}$. With increasing χ_n it is furthermore observed that the amplitude of the pressure perturbation decreases.

Result for $\omega_0 = 1$, $l = \frac{3}{2}\pi$ and $\chi_1 = \frac{1}{3}$: As for Case A, there is a special length of the vibrating wall for which the solution p_0^B cancels for $t \geq x + l$. For Case B this length is given by $l = \frac{3}{2}\pi$. Again this special situation can be used to compare the numerical result with the analytical approximation obtained from employing the method of stationary phase.

Fig.(10) shows the numerical result for Case B at location $x = 20.0522$, $y = 0.475$ and $z = 0.725$ for $l = \frac{3}{2}\pi$, $\omega_0 = 1$ and $\chi_n = \frac{1}{3}$. Additionally in the figure the analytic approximation has been presented. From the top figure of Fig.(10) the difference between the analytic and numerical results is hardly visible. From the bottom figure of Fig.(10), which shows a magnification of the results for $t \in [25, 60]$, the difference can be observed. Like observed for Case A, the approximation, obtained from applying the method of stationary phase, slightly underpredicts the amplitude, but the frequency shows very good agreement.

4.4 Case B, $M \neq 0$

In Fig.(11) the numerical results for $M = 0.1$ at microphone locations $x = 20.025$, $y = 0.525$, $z = 0.475$ and $x = -20.025$, $y = 0.475$, $z = 0.525$ are

presented. In addition, the analytical solution p_0 for $M = 0.1$ and $M = 0$, obtained for $x = 20.025$, are presented in Fig.(11). The two microphone locations are almost exactly symmetric with respect to the plane $x = 0$. From Fig.(11) it is observed that the analytical solution p_0^B, given by Eq.(22), shows perfect agreement with the numerical result at the same microphone location. Secondly it is observed that, with the result for $M = 0$ as reference, the amplitude of the pressure is larger downstream and smaller upstream of $x = 0$. The same behavior was observed for Case A with mean flow, presented in the preceding section.

Also for Case B with mean flow, the numerical results and analytical solution have been observed to show very good agreement.

5 Conclusion

The numerical and analytical results, which have been presented for two specific wall vibration velocity functions and for various combinations of parameters such as the angular vibration frequency, the length of the vibrating wall and the mean flow Mach-number, have been shown to be in very good agreement.

The presented analytical solution encompasses a plane wave solution, of which the analytical solution can be obtained in closed form, and an infinite number of 'diffracted waves' (waves affected by reflection, scattering, diffraction, etc.). For the diffracted waves only an approximate solution has been obtained employing the method of stationary phase.

Except for the plunging wall case in which resonance occurs, it appears that the plane wave solution, which is the leading term in the solution, captures most of the characteristics of the solution. Only near the vibrating wall segment the influence of the diffracted waves is significant.

6 Acknowledgement

This work was sponsored by the "Stichting Nationale Computerfaciliteiten" (National Computing Facilities Foundation, NCF) for the use of supercomputer facilities, with financial support from the "Nederlandse Organisatie voor Wetenschappelijk Onderzoek" (Netherlands Organization for Scientific Research, NWO).

In addition the authors would like to acknowledge TNO TPD for sponsoring the research in aeroacoustics in the Engineering Fluid Dynamics group of the University of Twente. The research presented in this paper has been carried out within the UT-TNO Sound & Vibrations Research Center.

References

[1] H.L. Atkins and C.W. Shu, 'Quadrature-free implementation of discontinuous galerkin method for hyperbolic equations', *AIAA Journal*, Vol. 36, pp. 775-782, 1998

[2] C.P.A. Blom, "Discontinuous galerkin method on tetrahedral elements for aeroacoustics", Ph.D.-thesis, University of Twente, September 2003.

[3] C.P.A. Blom, R. Hagmeijer and H.W.M. Hoeijmakers, "Analytical and numerical analysis of duct acoustics generated by a vibrating wall segment", *AIAA-Paper 2004-2941*, 10^{th} AIAA/CEAS Aeroacoustics Conference, Manchester, May 2004.

[4] D.G. Crighton, A.P. Dowling, J.E. Ffowcs Williams, M. Heckl and F.G. Leppington, "Modern methods in analytical acoustics", Lecture Notes, Springer-Verlag, London, 1996.

[5] D.S. Jones, "Acoustic and electromagnetic waves", Clarendon Press, Oxford, 1986.

[6] A.H.W.M. Kuijpers, S.W. Rienstra, G. Verbeek and J.W. Verheij, "The acoustic radiation of baffled finite ducts with vibrating walls", *Journal of Sound and Vibration*, Vol. 216, No. 3, pp. 461-493, 1998.

[7] P.M. Morse and H. Feshbach, "Methods of theoretical physics", Vol. I & II, McGraw-Hill Book Company, Inc., 1953.

[8] P.M. Morse and K.U. Ingard, "Theoretical acoustics", McGraw-Hill Book Company, 1968.

[9] A.D. Pierce, "Acoustics. an introduction to its physical principles and applications", Acoustical Society of America, New York, 1994.